Downloaded from on October 9, 2025 - Published by Cold Spring Harbor Laboratory Press

RESEARCH COMMUNICATION

A critical affinity window for IgSF proteins DIP-α and Dpr10 is required for proper motor neuron arborization

Davys H. Lopez,[1,2] Kevin D. Rostam,[2,3] Sumaira Zamurrad,[2] Shuwa Xu,[4] and Richard S. Mann[2,3,5]

[1]Department of Genetics and Development, Columbia University Irving Medical Center, New York, New York 10032, USA; [2]Mortimer B. Zuckerman Mind Brain Behavior Institute, Columbia University, New York, New York 10027, USA; [3]Department of Biochemistry and Molecular Biophysics, Columbia University, New York, New York 10032, USA; [4]Division of Biology and Biological Engineering, California Institute of Technology, Pasadena, California 91125, USA; [5]Department of Systems Biology, Columbia University Irving Medical Center, New York, New York 10032, USA

For neurons to establish the correct connections in animal nervous systems, interactions between cell adhesion molecules (CAMs), expressed presynaptically and postsynaptically, are thought to guide neurons to their targets. Here, we assess the role that affinity between two cognate CAMs—DIP-α and Dpr10—plays in establishing the leg neuromuscular system in *Drosophila*. If affinity decreases or, surprisingly, increases past certain thresholds, motor neuron (MN) terminal branches fail to be maintained. Live imaging during development shows that when affinities are aberrant, MN filopodia are unable to productively engage their muscle targets. Thus, CAM affinities are tuned to achieve proper neuronal morphology.

Supplemental material is available for this article.

Received April 16, 2025; revised version accepted July 24, 2025.

The development of locomotive circuits requires motor neurons (MNs) to arborize and synapse onto the correct muscles. To do this, neurons undergo axon guidance or pathfinding, in which axons navigate close to their cellular targets (Van Vactor et al. 1993; Moreland and Poulain 2022); synaptic specificity, where short-range interactions establish synaptic choice (Tan et al. 2015; Moreland and Poulain 2022); and branching and arborization (Grueber and Sagasti 2010; Gibson and Ma 2011). In all of these steps, cell adhesion molecules (CAMs) have been implicated as playing critical roles (Sanes and Zipursky 2020; Moreland and Poulain 2022). For example, CAMs that bind heterophilically and homophilically such as Beat-Ia and Sidestep have been described during axon pathfinding (Van Vactor et al. 1993; Sink et al. 2001; Siebert et al. 2009; Stoeckli 2018), molecules such as the L1 protein subfamily are needed for synaptic specificity (Ango et al. 2004; Ashrafi et al. 2014; Telley et al. 2016; Sanes and Zipursky 2020), and Dscam1 and protocadherins are needed for self-avoidance (Lefebvre et al. 2012; Tadros et al. 2016; Lemieux et al. 2021).

In *Drosophila*, DIPs (Dpr-interacting proteins) and Dprs (defective in proboscis extension response) comprise two interacting families within the immunoglobulin superfamily (IgSF) set of CAMs that are expressed by a subset of neurons and required for synaptic specificity (Carrillo et al. 2015; Ashley et al. 2019; Venkatasubramanian et al. 2019; Bornstein et al. 2021; Brovero et al. 2021). The DIP–Dpr interaction network has nine Dprs (each with two immunoglobulin [Ig] domains) that bind selectively to DIPs, which have 21 members (each with three Ig domains) (Özkan et al. 2013; Carrillo et al. 2015; Cosmanescu et al. 2018)

DIP-α in particular has a well-described role in the developing adult leg motor system. Using gene trap reporters into *DIP-α* (Venken et al. 2011; Venkatasubramanian et al. 2019), its expression was mapped to three MNs that target the long tendon muscle in the femur (αFe-ltm), the long tendon muscle in the tibia (αTi-ltm), and the tarsal depressor muscle in the tibia (αTi-tadm) (Fig. 1). In *DIP-α*-null mutant animals, the terminal axon branches of the αFe-ltm are absent in almost all samples, whereas those of the αTi-ltm are missing ∼70% of the time and those of the αTi-tadm are rarely absent. *dpr10* is expressed broadly by all muscles, and in *dpr10*-null animals, the three *DIP-α*-expressing MNs display the same phenotype as *DIP-α*-null animals. Live imaging during pupal stages, when stereotyped MN terminal branches find and form stable synapses onto the correct muscles, revealed that in the absence of DIP-α, MN axons still extend filopodia to the correct muscles but fail to arborize and eventually retract, resulting in adults with no terminal branches (Venkatasubramanian et al. 2019).

K_Ds for homophilic and heterophilic binding for DIP/Dpr pairs vary by >100-fold, ranging from <2 to >200 µM (Cosmanescu et al. 2018; Xu et al. 2022). Interestingly, DIP-α and Dpr10 have among the strongest pairwise affinity in the DIP–Dpr interactome, with a K_D of 1.4 µM (Cosmanescu et al. 2018; Xu et al. 2022). Motivated by these observations, a series of mutations were knocked into *DIP-α* and *dpr10* loci to either decrease or increase affinity at the DIP-α–Dpr10 binding interface (Xu et al. 2022). In the optic lobe, it was shown that reducing the affinity of either *DIP-α* or *dpr10* causes loss-of-function phenotypes such as synaptic mistargeting and cell death and that the severity of these phenotypes scales with the magnitude of affinity reduction (Xu et al. 2022). Interestingly, increasing affinity did not alter targeting but did affect cell survival in this system. Although these results indicate that affinity is tuned to achieve proper cell survival and synaptic wiring in the visual system (Xu et al. 2022), no effect on leg MN survival has been observed in *DIP-α* and *dpr10* mutants. This may be because in the fly visual

[*Keywords*: DIPs and Dprs; *Drosophila melanogaster*; IgSF; axon arborization; cell adhesion molecules; live imaging; motor neuron; muscle targeting; neural development]
Corresponding author: rsm10@columbia.edu
Article published online ahead of print. Article and publication date are online at http://www.genesdev.org/cgi/doi/10.1101/gad.352936.125. Freely available online through the *Genes & Development* Open Access option.

© 2025 Lopez et al. This article, published in *Genes & Development*, is available under a Creative Commons License (Attribution-NonCommercial 4.0 International), as described at http://creativecommons.org/licenses/by-nc/4.0/.

Downloaded from on October 9, 2025 - Published by Cold Spring Harbor Laboratory Press

system, neurons are produced in excess, and those that do not form functional synapses undergo apoptosis (Courgeon and Desplan 2019). In contrast, each leg MN has a hardwired muscular target and morphology (Enriquez et al. 2015; Guan et al. 2022).

Here, we took advantage of the stereotyped leg neuromuscular system to examine the role of affinity between DIP-α and Dpr10. We found that decreasing or increasing affinity does not affect cell survival or cause mistargeting but rather has a role in stabilizing MN axon arborization. Using a quantitative neuron tracing analysis (Arshadi et al. 2021), we found that the three *DIP-α*-expressing MNs (αMNs) have different affinity requirements and that alterations to affinity impact locomotion. Surprisingly, we found that increasing affinity also impairs terminal branching. Together, these results reveal that affinities between interacting CAMs have been tuned to achieve proper neuronal development.

Results and Discussion

Live imaging of leg MN arborization during pupal development

Previous work established a live-imaging protocol to image the three *DIP-α*-expressing MNs (αMNs) until ~45 h after pupal formation (APF) (Venkatasubramanian et al. 2019). To capture axon morphology changes between mid-pupa and adult, we extended this protocol to visualize later pupal stages. We used *DIP-α-T2A-Gal4>20-XUAS-6XGFP* to visualize the three αMNs together with *Mef2-QF>QUAS-10XmCherry* to visualize muscles as they develop from ~20 to 108 h APF, which encompasses almost all of pupal development (Fig. 1A; Supplemental Videos S1, S3). Using this setup, we were limited to visualizing MNs and muscles in the tibia (αTi-MNs), which is close to the surface of the pupa.

As early as 20 h APF, αTi-MNs have already targeted nascent clusters of myoblasts within the tibia, as described previously (Venkatasubramanian et al. 2019). By visualizing the developing myoblasts with myr::tdTomato, we found that the myoblasts are organized into interconnected clusters that will become future muscle groups; that is, the tibia tarsal depressor muscle (Ti-tadm) and the tibia long tendon muscle (Ti-ltm) (Supplemental Video S2; Supplemental Fig. S3). These clusters then split and become discrete muscle groups. Between 25 and 55 h APF, myoblasts fuse and become syncytial multifiber muscles (Fig. 1B). By 20–60 h APF, the videos show single mobile myoblasts that join and fuse with a particular muscle fiber (Fig. 1B). At ~50 h APF, αTi-MNs have reached and stabilized a nascent axon terminus with a limited number of branches on their targeted muscle. From ~50 h APF onward, this initial nascent axon terminus will continue to give rise to new branches and elongate its existing branches until a few hours before the animal ecloses (Fig. 1B). During this later phase, the movement of the αMN filopodia slows and transitions to synapse formation (Supplemental Video S1). Based on these observations, there are at least two different phases of axon morphogenesis: an initial phase where the αTi-MNs choose and stabilize muscle fibers as they are developing and a second phase when αTi-MNs limit their mobility but continue to arborize while forming synapses. This indicates that MN arborization occurs for much longer than previously noted (Venkatasubramanian et al. 2019).

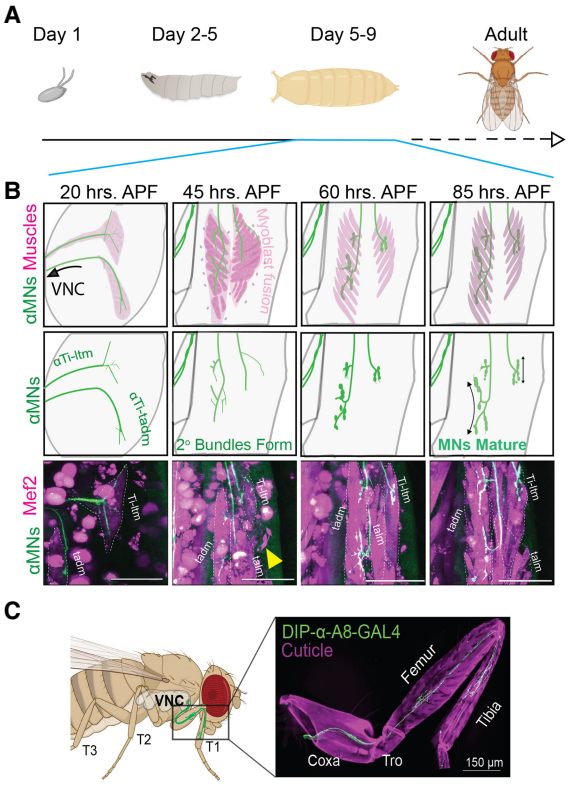

Figure 1. Overview of fly leg MN arborization. (*A*) Life cycle of *Drosophila*. Imaging was done over most of pupal development, from 20 h after pupal formation (APF) onward. (*B*) Drawings and individual frames from videos of *DIP-α-T2A-Gal4>>20XUAS-6XGFP, Mef2-QF>>10XQUAS-6XmCherry* flies. The first row shows αMNs in green and muscles in magenta. The sequence shows αMNs developing in the context of myoblast fusion. The second row shows developing αMNs. At early time points, αMNs are more mobile. From 60 h APF onward, axon termini begin to stabilize but continue to mature until eclosion. The third row shows stills from Supplemental Video S1. (*C*) Adult fly (*left*) and leg (*right*). αMNs, visualized here with *A8-Gal4, 20XUAS-6XGFP*, are born in the VNC and extend to arborize in the tibia and femur. (Ti-ltm) Tibia long tendon muscle, (tadm) tarsal depressor muscle, (talm) tarsal levator muscle.

Reducing DIP-α affinity to Dpr10 impedes arborization

We examined the role of affinity on leg MN arborization using alleles in *DIP-α* and *dpr10* that change the strength of their interaction based on biophysical measurements (Xu et al. 2022). These alleles alter the affinity between DIP-α and Dpr10 in graded fashion over a wide range, do not affect binding specificity, and do not alter homophilic binding between DIP-α and itself. We used the *DIP-α* mutants K81Q (K_D = 31.8 µM, *DIP-α*$^{-20F}$; superscripts indicate the direction and fold change [F] in affinity relative to wild type) and both K81Q and G74S (K_D = 68.0 µM, *DIP-α*$^{-50F}$) (Fig. 2A) and *dpr10* mutants V144K (K_D = 11.3 µM, *dpr10*$^{-8F}$), Q138D (K_D = 27.6 µM, *dpr10*$^{-20F}$), and G99D, Q142E, and V144K in combination (K_D = 50.0 µM, *dpr10*$^{-40F}$) (Fig. 3A). Although we could not monitor expression levels of these alleles in legs by antibody staining, they were expressed in the correct patterns and levels in

Downloaded from on October 9, 2025 - Published by Cold Spring Harbor Laboratory Press

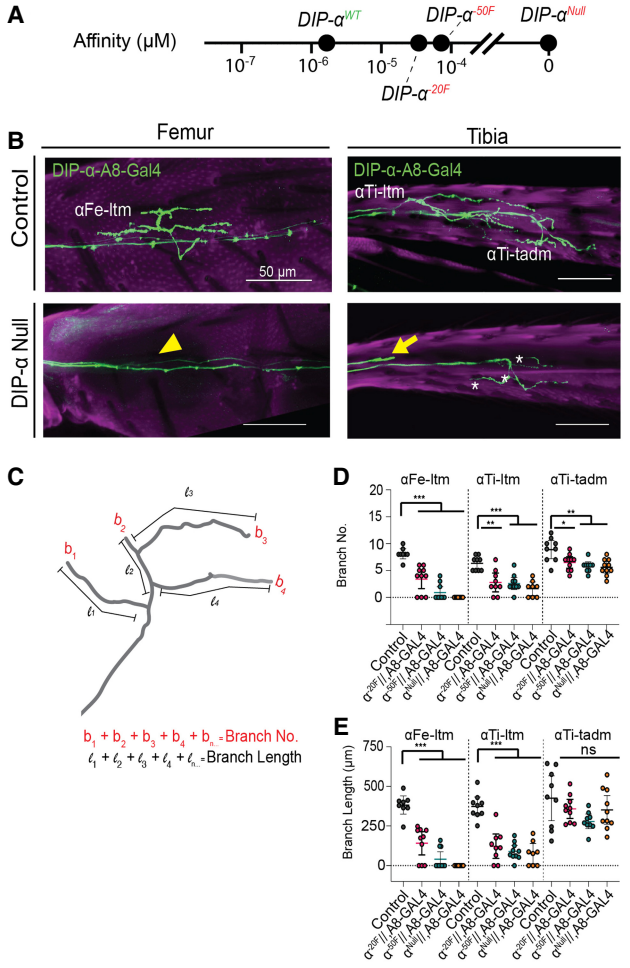

Figure 2. Analysis of *DIP-α* alleles with reduced affinity. (*A*) Affinity range of *DIP-α* mutants in log scale. (*B*) Representative femur and tibia images of *yw, A8-Gal4>>20XUAS-6XGFP* (control) and *DIP-α*^{Null}*//; A8-Gal4>>20XUAS-6XGFP* femur and tibia leg segments. (*C*) Schematic of how MN morphologies were quantified. (*D*) Quantification of terminal branch number using *A8-Gal4* as the readout. αFe-ltm: control, $n = 8$; *DIP-α*$^{-20F}$*//*, $n = 10$; *DIP-α*$^{-50F}$*//*, $n = 10$; *DIP-α*^{Null}*//*, $n = 10$. αTi-ltm: control, $n = 9$; *DIP-α*$^{-20F}$*//*, $n = 9$; *DIP-α*$^{-50F}$*//*, $n = 10$; *DIP-α*^{Null}*//*, $n = 8$. αTi-tadm: control, $n = 9$; *DIP-α*$^{-20F}$*//*, $n = 10$; *DIP-α*$^{-50F}$*//*, $n = 9$; *DIP-α*^{Null}*//*, $n = 10$. (*E*) Quantification of total branch length using *A8-Gal4* as the readout. αFe-ltm: control, $n = 8$; *DIP-α*$^{-20F}$*//*, $n = 10$; *DIP-α*$^{-50F}$*//*, $n = 10$; *DIP-α*^{Null}*//*, $n = 10$. αTi-ltm: control, $n = 9$; *DIP-α*$^{-20F}$*//*, $n = 9$; *DIP-α*$^{-50F}$*//*, $n = 10$; *DIP-α*^{Null}*//*, $n = 9$. αTi-tadm: control, $n = 9$; *DIP-α*$^{-20F}$*//*, $n = 10$; *DIP-α*$^{-50F}$*//*, $n = 9$; *DIP-α*^{Null}*//*, $n = 10$.

the medulla of the pupal optic lobe (Xu et al. 2022). The αMNs were visualized using a previously characterized transcriptional enhancer isolated from *DIP-α* called A8 fused to Gal4 (*A8-Gal4*) (Fig. 1; Venkatasubramanian et al. 2019) and were repeated using a MiMIC line converted to T2A-Gal4 (Supplemental Fig. S1). To acquire quantitative information regarding branch number and branch length, we traced and quantified both parameters using FIJI semiautomated tracing software (Arshadi et al. 2021). We compared control animals with wild-type alleles versus animals homozygous for the *DIP-α* allele with *A8-Gal4* (Fig. 2) or one copy of the mutant *DIP-α* allele and one copy of the *DIP-α-T2A-Gal4* (which is a strong hypomorph) (Supplemental Fig. S1; Venkatasubramanian et al. 2019) . Animals with null alleles served as a negative control.

Compared with controls, adults with reduced *DIP-α* affinity (*DIP-α*$^{-20F}$ and *DIP-α*$^{-50F}$) show phenotypes similar to *DIP-α*-null animals, where αMN axons fail to arborize onto their muscle target and have no terminal branches (Fig. 2D). Using *A8-Gal4* to compare the three αMNs, we found that these MNs have different expressivities in the absence of *DIP-α* or *dpr10*: The αFe-ltm completely fails to arborize, αTi-ltm terminal branches are reduced or lost in ~70%–80% of animals, and the αTi-tadm is rarely affected (Venkatasubramanian et al. 2019). In addition to these observations with null alleles, we also found a graded affinity requirement for each of the αMNs. For instance, we found that the αFe-ltm has less arborization with the *DIP-α*$^{-50F}$ allele compared with the *DIP-α*$^{-20F}$ allele, suggesting that the affinity required to fully stabilize the branch is greater than −20F (Fig. 2D,E). The αTi-ltm also fails to arborize, though the expressivity is not as strong as in the αFe-ltm (Fig. 2D,E). Finally, although the αTi-tadm rarely shows a complete loss of arborization, both branch number and branch length are reduced (Fig. 2D,E; Supplemental Fig. S1B,C). Together, these data reveal that the three αMNs all require different minimal affinities to properly arborize onto their target muscles.

Reducing Dpr10 affinity to DIP-α impedes arborization

As with the *DIP-α* alleles, we examined homozygous *dpr10* alleles with reduced affinity mutations using both *A8-Gal4* and *DIP-α-T2A-GAL4* as readouts of αMN morphology. Using the *A8-Gal4* readout with *dpr10*$^{-8F}$, we found that αFe-ltm branches are not completely absent but demonstrate a decrease in branch number and length, whereas the *dpr10*$^{-20F}$ allele results in the complete loss of terminal branches in this MN (Fig. 3C,D). For the αTi-ltm, the complete absence of arborization occurs at a lower frequency compared with the αFe-ltm for all *dpr10* alleles, indicating that the αFe-ltm has a higher affinity requirement than the αTi-ltm (Fig. 3C,D). In contrast, using *DIP-α-T2A-Gal4*, the αTi-ltm fails to arborize in most *dpr10*$^{-8F}$ animals (Supplemental Fig. S1E,F). This discrepancy may be because *DIP-α-T2A-Gal4* is a strong hypomorph of *DIP-α* (Venkatasubramanian et al. 2019), possibly resulting in lower levels of DIP-α and a compromised interaction between αMNs and muscles. For the αTi-tadm, there is a slight decrease in branch number and length in both readouts, and in both cases, the αTi-tadm arborization phenotype is less strong than in the αTi-ltm (Fig. 3C,D; Supplemental Fig. S1E,F).

Together, these results suggest that the affinity requirement for the arborization of the αFe-ltm is higher than the αTi-ltm, consistent with the differences observed in expressivity for *DIP-α-* and *dpr10*-null alleles. The αTi-tadm is rarely fully lost in either *DIP-α-* or *dpr10*-null alleles, indicating that it likely relies on additional molecules to achieve proper morphology. Finally, these results indicate that reducing the affinity of the postsynaptic CAM has the same effects as reducing the affinity of the presynaptic CAM.

Increasing affinity also impedes αMN arborization

Given the loss of arborization when the DIP-α::Dpr10 affinity was reduced, we considered the possibility that

Downloaded from on October 9, 2025 - Published by Cold Spring Harbor Laboratory Press

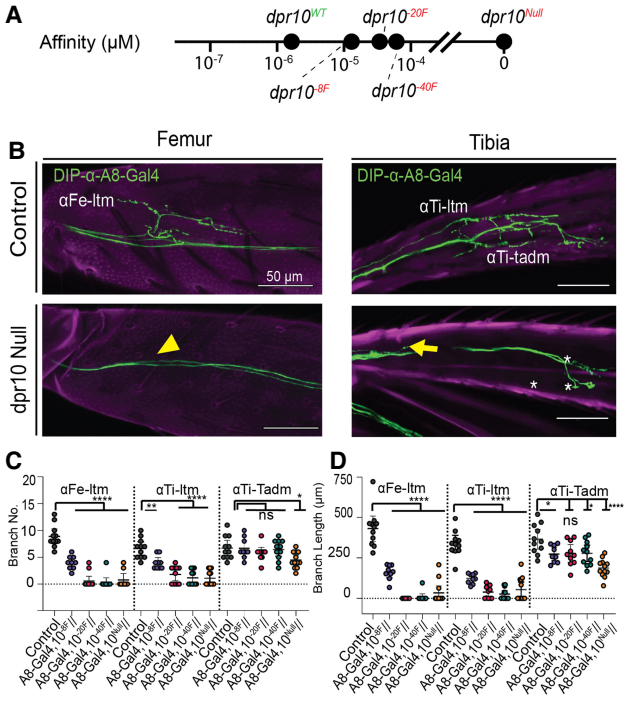

Figure 3. Analysis of *dpr10* alleles with reduced affinity. (*A*) Affinity range of *dpr10* mutants in log scale. (*B*) Representative images of *yw, A8-Gal4>>20XUAS-6XGFP* (control) and *A8-Gal4, dpr6^{Null}, dpr10^{Null}//, >>20XUAS-6XGFP* femur and tibia leg segments. (*C*) Quantification of terminal branch number using *A8-Gal4* as the readout. αFe-ltm: control, $n = 11$; *dpr6^{Null}, dpr10^{-8F}//*, $n = 9$; *dpr6^{Null}, dpr10^{-20F}//*, $n = 10$; *dpr6^{Null}, dpr10^{-40F}//*, $n = 11$; *dpr6^{Null}, dpr10^{Null}//*, $n = 12$. αTi-ltm: control, $n = 11$; *dpr6^{Null}, dpr10^{-8F}//*, $n = 9$; *dpr6^{Null}, dpr10^{-20F}//*, $n = 10$; *dpr6^{Null}, dpr10^{-40F}//*, $n = 11$; *dpr6^{Null}, dpr10^{Null}//*, $n = 12$. αTi-tadm: control, $n = 11$; *dpr6^{Null}, dpr10^{-8F}//*, $n = 9$; *dpr6^{Null}, dpr10^{-20F}//*, $n = 10$; *dpr6^{Null}, dpr10^{-40F}//*, $n = 10$; *dpr6^{Null}, dpr10^{Null}//*, $n = 12$. (*D*) Quantification of total branch length using *A8-Gal4* as the readout. αFe-ltm: control, $n = 11$; *dpr6^{Null}, dpr10^{-8F}//*, $n = 9$; *dpr6^{Null}, dpr10^{-20F}//*, $n = 10$; *dpr6^{Null}, dpr10^{-40F}//*, $n = 11$; *dpr6^{Null}, dpr10^{Null}//*, $n = 12$. αTi-ltm: control, $n = 11$; *dpr6^{Null}, dpr10^{-8F}//*, $n = 9$; *dpr6^{Null}, dpr10^{-20F}//*, $n = 10$; *dpr6^{Null}, dpr10^{-40F}//*, $n = 11$; *dpr6^{Null}, dpr10^{Null}//*, $n = 12$. αTi-tadm: control, $n = 11$; *dpr6^{Null}, dpr10^{-8F}//*, $n = 9$; *dpr6^{Null}, dpr10^{-20F}//*, $n = 10$; *dpr6^{Null}, dpr10^{-40F}//*, $n = 11$; *dpr6^{Null}, dpr10^{Null}//*, $n = 12$. For all graphs, statistical significance was determined using an unpaired nonparametric two-tailed Mann–Whitney test. Error bars represent mean with 95% confidence intervals. (ns) No statistical difference, (*) $P < 0.05$, (**) $P < 0.01$, (****) $P < 0.0001$. All quantifications were done with *20XUAS-6XGFP*.

increasing affinity might result in more and/or longer branches. To address this, we used the following *DIP-α* and *dpr10* mutants: *DIP-α^{G74A}* ($K_D = 0.90$ μM, *DIP-α^{+2F}*) and *dpr10^{Q142M}* ($K_D = 0.19$ μM, *dpr10^{+10F}*). In addition, we also analyzed the combination of *DIP-α^{+2F}* and *dpr10^{+10F}*, which results in an increased affinity of +15F (*DIP-α* and *dpr10^{+15F}*, $K_D = 0.10$ μM) (Fig. 4A). We found that in *DIP-α^{+2F}* animals with *DIP-α-T2A-Gal4*, αMN branch number and length are not affected (Fig. 4C). However, in *dpr10^{+10F}* flies, αTi-ltm and αTi-tadm branch number and branch length were on average shorter than in control flies (Fig. 4C,D). In *DIP-α* and *dpr10^{+15F}* flies, some αTi-ltm and αTi-tadm axons completely fail to arborize. Together, these results show that increasing affinity, like reducing affinity, also adversely affects terminal branch arborization. We note, however, that when using *A8-Gal4* as the readout, the lack of arborization phenotype is not as strong as in experiments done with *DIP-α-T2A-Gal4*, even in a sensitized

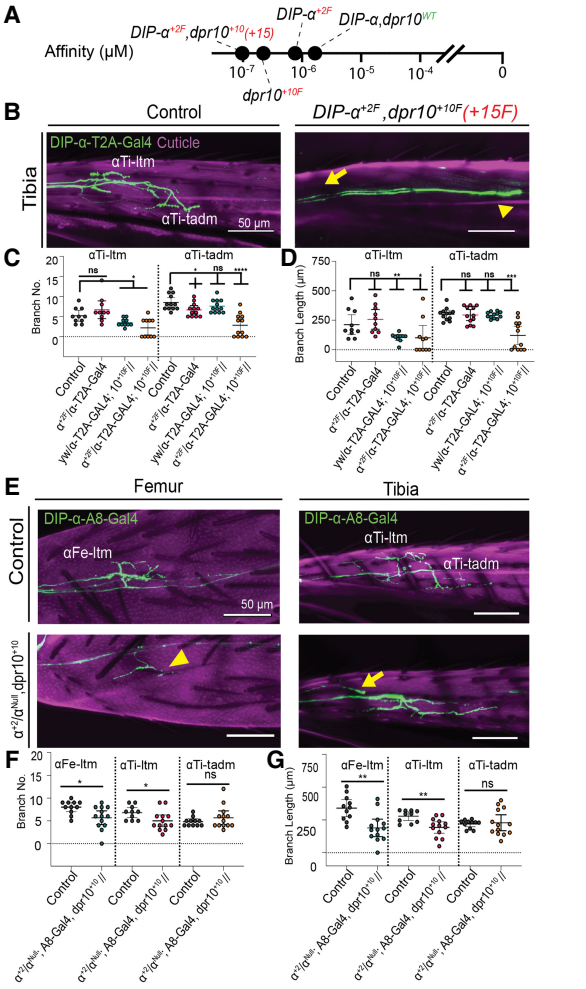

Figure 4. Analysis of increased affinity genotypes. (*A*) Affinity range of increased affinity mutants in log scale. (*B*) Representative images of *yw/DIP-α-T2A-Gal4>>20XUAS-6XGFP* (control) and *DIP-α^{+2F}/DIP-α-T2A-Gal4; dpr6^{Null}, dpr10^{+10}//>>20XUAS-6XGFP (+15F)* tibia segments. (*C*) Quantification of terminal branch number using *DIP-α-T2A-Gal4* as the readout. αTi-ltm: control, $n = 10$; *DIP-α^{+2F}*, $n = 10$; *dpr10^{+10F}*, $n = 10$; *DIP-α^{+2F}* and *dpr10^{+10F}*, $n = 10$. αTi-tadm: control, $n = 12$; *DIP-α^{+2F}*, $n = 12$; *dpr10^{+10F}*, $n = 12$; *DIP-α^{+2F}* and *dpr10^{+10F}*, $n = 12$. (*D*) Quantification of total branch length using *DIP-α-T2A-Gal4* as the readout. αTi-ltm: control, $n = 10$; *DIP-α^{+2F}*, $n = 10$; *dpr10^{+10F}*, $n = 10$; *DIP-α^{+2F}* and *dpr10^{+10F}*, $n = 10$. αTi-tadm: control, $n = 12$; *DIP-α^{+2F}*, $n = 12$; *dpr10^{+10F}*, $n = 12$; *DIP-α^{+2F}* and *dpr10^{+10F}*, $n = 12$. For all graphs, statistical significance was determined using an unpaired nonparametric two-tailed Mann–Whitney test. Error bars represent mean with 95% confidence intervals. (ns) No statistical difference, (*) $P < 0.05$, (**) $P < 0.01$, (***) $P < 0.001$, (****) $P < 0.0001$. (*E*) Representative images of control, *yw/DIP-α^{Null}; A8-Gal4, dpr6^{Null}, dpr10^{Q142M}/+>>20XUAS-6XGFP*, and *DIP-α^{+2}/DIP-α^{Null}; A8-Gal4; dpr6^{Null}, dpr10^{+10}//>>20XUAS-6XGFP* femur and tibia leg segments. (*F*) Quantification of terminal branch number using *A8-Gal4* as the readout. αFe-ltm: control, $n = 11$; *DIP-α^{+2}/DIP-α^{Null}; dpr6^{Null}, dpr10^{+10}//*, $n = 13$. αTi-ltm: control, $n = 10$; *DIP-α^{+2}/DIP-α^{Null}; dpr6^{Null}, dpr10^{+10}//*, $n = 13$. αTi-tadm: control, $n = 11$; *DIP-α^{+2}/DIP-α^{Null}; dpr6^{Null}, dpr10^{+10}//*, $n = 13$. (*G*) Quantification of total branch length using *A8-Gal4* as the readout. αFe-ltm: control, $n = 11$, *DIP-α^{+2}/DIP-α^{Null}, dpr6^{Null}dpr10^{+10}//*, $n = 13$. αTi-ltm: control, $n = 10$; *DIP-α^{+2}/DIP-α^{Null}, dpr6^{Null}, dpr10^{+10}//*, $n = 14$. αTi-tadm: control, $n = 11$; *DIP-α^{+2}/DIP-α^{Null}; dpr6^{Null}, dpr10^{+10}//*, $n = 13$. For all graphs, statistical significance was determined using an unpaired nonparametric two-tailed Mann–Whitney test. Error bars represent mean with 95% confidence intervals. (ns) No statistical difference, (*) $P < 0.05$, (**) $P < 0.01$. All quantifications were done with *20XUAS-6XGFP*.

Downloaded from on October 9, 2025 - Published by Cold Spring Harbor Laboratory Press

background with only one functional copy of *DIP-α* (*DIP-α^{+2F}/DIP-α^{Null}* and *dpr10^{+10F}//*). Nevertheless, there is a reduction in branch number and branch length for both the αFe-ltm and αTi-ltm in this genotype (Fig. 4F,G). We also expressed the marker Bruchpilot (Brp-short::mStraw) (Mosca and Luo 2014) in *DIP-α* and *dpr10^{+15F}* and control flies to determine whether MNs with reduced branches can still form synapses. We found that in *DIP-α* and *dpr10^{+15F}* flies, the αTi-ltm and αTi-tadm have Brp puncta, indicating that they are still able to assemble synapses (Supplemental Fig. S2).

These experiments indicate that when the affinity between DIP-α and Dpr10 is increased above a certain threshold, arborization defects result, but the penetrance of this effect depends on the status of the *DIP-α* locus. For example, it is possible that a truncated DIP-α protein generated by the *DIP-α-T2A-Gal4* allele is further sensitizing the phenotype.

Increasing affinity prevents the stabilization of developing αMNs

We next used our live-imaging protocol to compare αMN development from ~25 to 80 h APF in control (*yw/DIP-α-T2A-Gal4*) and experimental (*DIP-α-T2A-Gal4; DIP-α* and *dpr10^{+15F}*) flies, the time window when αMN branches stabilize on their muscle targets (Supplemental Video S2; Venkatasubramanian et al. 2019). By ~25 h APF in control animals, both the αTi-ltm and the αTi-tadm have already reached their muscle targets. Between 35 and 55 h APF, axons branch and extend filopodia in the general area of their muscle targets. At ~60 h APF, some filopodia will stabilize. In *DIP-α* and *dpr10^{+15F}* animals, both the αTi-ltm and the αTi-tadm reach their muscle targets successfully at 24 h APF. Very few differences can be seen in the next 24 h. However, at 60 h APF, multiple aberrant tertiary branches have extended but fail to stabilize and instead retract, resulting in the branchless phenotype observed in the adult. Interestingly, this is similar to what has been described for *DIP-α* nulls (Fig. 5A). These results indicate that αMNs can initially find the correct muscle target and send out filopodia to the correct myoblast cluster but fail to maintain the interaction long enough for the axons to fully arborize.

Although loss of arborization in increased affinity mutants was initially surprising, we have recently shown that *dpr10* is also expressed by αMNs and that removing *dpr10* in MNs leads to abnormally long branches in both the αTi-ltm and αTi-tadm (Morano et al. 2025). Therefore, a possible mechanism that contributes to the loss of branching in the *DIP-α* and *dpr10^{+15F}* mutant is that the higher-affinity interaction between DIP-α and Dpr10 is occurring in *cis* (in MNs), which competes with DIP-α's ability to interact with Dpr10 in *trans* in muscle cells. This could explain why the filopodia still extend and target the correct muscles but are not able to "anchor" long enough to generate stable terminal branches. *dpr10* is also expressed by other MNs in addition to the αMNs. Therefore, another plausible explanation is that DIP-α in αMNs is interacting with Dpr10 present in other MNs. However, this seems less likely, as we would expect the filopodia to become less mobile in the *DIP-α* and *dpr10^{+15F}* mutant due to greater interneuronal contact, which was not observed in live imaging (Supplemental Video S2).

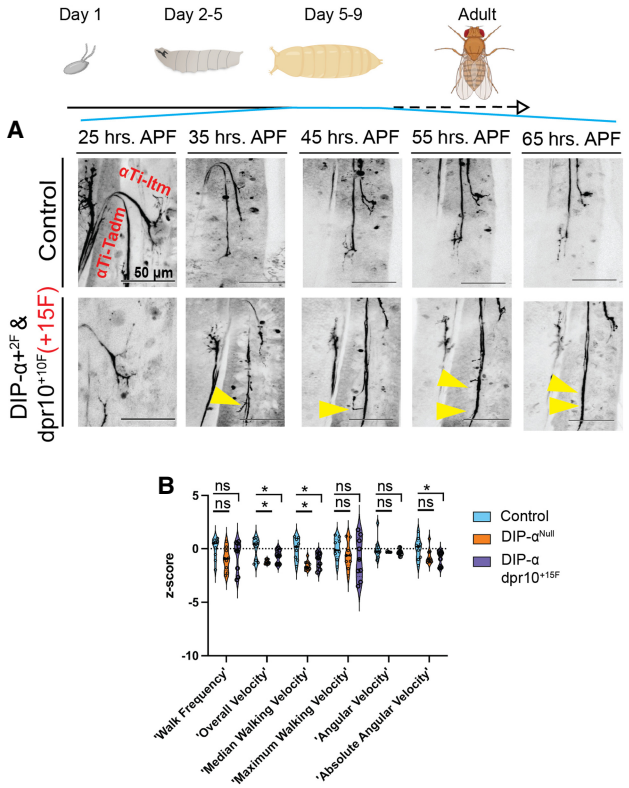

Figure 5. Live imaging and locomotion analysis. (*A*) Still images of a time-lapse video (see Supplemental Video S2) of *yw/DIP-α-T2A-Gal4>>20XUAS-6XGFP* pupa (*top* row) and *DIP-α^{G74A}/DIP-α-T2A-Gal4; dpr6^{Null}, dpr10^{Q142M}//>>20XUAS-6XGFP (+15F)* flies (*bottom* row). Yellow arrowheads point to small filopodia that aberrantly extend but ultimately retract in *DIP-α^{G74A}/DIP-α-T2A-Gal4; dpr6^{Null}dpr10^{Q142M}//* MNs. (*B*) Walking parameters measured in control (*yw, 20XUAS-6XGFP*), *DIP-α^{Null}//, 20XUAS-6XGFP*, and +15F gain-of-affinity *DIP-α^{G74A}//20XUAS-6XGFP;dpr6^{Null}, dpr10^{Q142M}(+15)//* genotypes. Control, $n = 10$; *DIP-α$^{Nul\ l}$*, $n = 10$; *DIP-α* and *dpr10^{+15F}*, $n = 10$. (*) $P < 0.05$.

Another relevant observation is that, like the time-lapse videos of *DIP-α^{Null}* animals (Venkatasubramanian et al. 2019), the live-imaging videos of *DIP-α* and *dpr10^{+15F}* mutants reveal that filopodia still extend to the correct muscle but are unable to make stable contacts with their target and then retract (Fig. 5A; Supplemental Video S2). This reinforces the idea that DIP-α::Dpr10 *trans* interactions are needed to stabilize terminal branches and not for axon guidance or synaptic specificity. Furthermore, this suggests that there must be additional mechanisms that help MN axons recognize their targets. We propose that the proper DIP-α::Dpr10 affinity range is needed to stabilize the contact long enough to recruit more DIP-α::Dpr10 *trans* interactions, which promote further arborization.

Changing affinity leads to behavioral defects

Using a free walking behavioral assay that reports various walking parameters (Howard et al. 2019), we compared the highly penetrant *DIP-α^{Null}* and *DIP-α* and *dpr10^{+15F}* alleles with control animals. Both *DIP-α^{Null}* and *DIP-α* and *dpr10^{+15F}* flies have reduced overall velocity and median

Downloaded from on October 9, 2025 - Published by Cold Spring Harbor Laboratory Press

walking velocity. Furthermore, *DIP-α* and *dpr10*$^{+15F}$ flies also have a reduced absolute angular velocity compared with controls (Fig. 5B). Although it is possible that these effects are the result of other, non-MN *DIP-α*-expressing neurons elsewhere in the nervous system, they demonstrate that changing the affinity between DIP-α::Dpr10 adversely affects locomotion as well as axon branching.

The role that affinity plays in DIP-α::Dpr10 function in vivo

Our data show that a limited affinity range is required for DIP-α::Dpr10 to establish a normal terminal arborization morphology. We suggest that the role of this interaction is to bring the presynaptic and postsynaptic membranes together long enough to nucleate more *trans* interactions via either additional DIP-α::Dpr10 interactions or other unknown CAMs that subsequently assemble during arborization. Accordingly, decreasing the DIP-α::Dpr10 affinity below a threshold is likely to decrease the overall avidity of the MN–muscle contact. This would disrupt the subsequent oligomerization of DIP-α::Dpr10 on the two membranes that are needed for arborization. New tools that fluorescently tag DIP-α in vivo could help to further elucidate these mechanisms (Rostam et al. 2025).

The range of affinities among the DIP–Dpr family is surprisingly large. For instance, the K_D between DIP-β and Dpr10 is 55 μM, the K_D between DIP-κ and Dpr6 is 286 μM, and the K_D between DIP-α and Dpr10 is <2 μM. Our results raise the question of why some DIPs and Dprs have relatively low binding affinities and how they are functional. One answer may be that low-affinity interactions are either nonfunctional or play a modest role by supplementing higher-affinity interactions between other interacting proteins. Alternatively, local receptor concentrations can turn weak dissociation constants into substantial binding. For example, receptor compartmentalization (Hyman et al. 2014) or cooperative binding via the receptor or ligand (Honig and Shapiro 2020) or through a coreceptor (Kondo et al. 2024) can all contribute to an increase in effective avidity in vivo. However, increasing affinity, as shown here, can also have adverse effects. Therefore, for any pair of CAMs, the overall avidity has likely evolved to optimize the strength (or duration) of the interaction.

Materials and methods

Fly stocks

All fly stocks were described previously by Venkatasubramanian et al. (2019) and Xu et al. (2022). All chromosomes with mutant *dpr10* alleles also had a null mutation in *dpr6*, which was not expressed in the adult muscles and did not play a role in αMN targeting (Venkatasubramanian et al. 2019). In genotypes where *A8-Gal4* was used to drive GFP, it was homozygous.

Dissection and microscopy

For adult leg dissection, flies were first immersed in 70% ethanol for ∼1 min and rinsed three times in 0.3% Triton-X in PBS. Abdomens and heads were then removed, and legs attached to thoraxes were fixed overnight at 4°C in 4% paraformaldehyde in 0.3% Triton-X in PBS. The next day, legs and thoraxes were washed five times in 0.3% Triton-X in PBS and then stored in 80% VectaShield in PBS overnight at 4°C. Legs were removed from the thoraxes and placed onto a glass slide in a drop of VectaShield mounting medium (Vector Laboratories). Coverslips (18 mm × 18 mm) were then placed on top with dental wax on the corners to prevent the coverslips from crushing the legs. Sections (0.5 μm thick) in the *Z*-axis were imaged using a Zeiss LSM 800 confocal laser scanning microscope.

Motor neuron axon branch quantification and statistical analysis

To quantify leg motor neurons, only one T1 leg from each animal was imaged, and their neurons were traced using the simple neuron tracer from ImageJ (Arshadi et al. 2021). For each neuron, with the exception of the αTi-tadm, the tracing began at the first bifurcation point. For the αTi-tadm, only the most distal branch was traced due to the presence of collateral branches that would have misrepresented the terminal branch number and branch length. Both the total terminal branch number and the sum of the cable length values were separately plotted and analyzed using GraphPad Prism 9.0. For all graphs, statistical significance was determined using an unpaired nonparametric two-tailed Mann–Whitney test. Error bars in the figures represent mean with 95% confidence intervals, and significance is indicated as follows: no statistical difference (ns), $P < 0.05$ (*), $P < 0.01$ (**), $P < 0.001$ (***), and $P < 0.0001$ (****).

Live imaging of MN development in pupae

Pupae were staged by picking late (wandering) L3 larva and placing them in a separate vial with a moist tissue, kept at 25°C, and then picked 24 h later. A small window on the left ventral side of the pupal case was made using forceps to expose just the T1 leg. Individual pupae were placed on a glass slide, surrounded by two layers of filter paper dampened with distilled water. A 5 μL drop of distilled water was placed at the center of a glass coverslip (N-1.5) and placed exactly over the exposed T1 leg. Petroleum jelly surrounding the filter paper was used to seal the space between the coverslip and the glass slide to retain humidity. Samples were imaged on a Zeiss LSM 800 microscope with 25× objective, with a 10 min interval between each *z*-stack series. Videos were generated using FIJI software (Schneider et al. 2012) at 5 fps.

Behavior

The fly arena setup was described by Howard et al. (2019). All behavior videos were recorded during the morning activity peak time (9:00 a.m. to 12:00 p.m.). Each recorded video had 10 flies. Videos were recorded at a rate of 30 fps and stored in a compressed "fly format" using software

Downloaded from on October 9, 2025 - Published by Cold Spring Harbor Laboratory Press

written by Andrew Straw at the University of Freiburg. Videos were tracked using the MATLAB-based FlyTracker software from the California Institute of Technology Vision Laboratory (Eyjolfsdottir et al. 2014). Video data were analyzed using MATLAB scripts as described previously (Howard et al. 2019).

Competing interest statement

The authors declare no competing interests.

Acknowledgments

We thank members of the Mann laboratory for feedback and advice during this project, Lalanti Venkatasubramanian for mentoring, Kai Zinn for reagents, and Larry Shapiro, Alina Sergeeva, Ulrich Hengst, Wes Grueber, and Nick Morano for discussions and suggestions. This work was supported by a grant from the National Institute of Neurological Disorders and Stroke to R.S.M. (R01NS070644).

Author contributions: D.H.L. conceived the project, acquired and analyzed the data, and wrote and edited the manuscript. K.D.R. acquired and analyzed the data and edited the manuscript. S.Z. acquired and analyzed the data. S.X. provided reagents and edited the manuscript. R.S.M. conceived the project, analyzed the data, wrote and edited the manuscript, and acquired the project funding.

References

Ango F, Di Cristo G, Higashiyama H, Bennett V, Wu P, Huang ZJ. 2004. Ankyrin-based subcellular gradient of neurofascin, an immunoglobulin family protein, directs GABAergic innervation at Purkinje axon initial segment. *Cell* **119:** 257–272. doi:10.1016/j.cell.2004.10.004

Arshadi C, Günther U, Eddison M, Harrington KIS, Ferreira TA. 2021. SNT: a unifying toolbox for quantification of neuronal anatomy. *Nat Methods* **18:** 374–377. doi:10.1038/s41592-021-01105-7

Ashley J, Sorrentino V, Lobb-Rabe M, Nagarkar-Jaiswal S, Tan L, Xu S, Xiao Q, Zinn K, Carrillo RA. 2019. Transsynaptic interactions between IgSF proteins DIP-α and Dpr10 are required for motor neuron targeting specificity. *eLife* **8:** 1–24. doi:10.7554/eLife.42690

Ashrafi S, Betley JN, Comer JD, Brenner-Morton S, Bar V, Shimoda Y, Watanabe K, Peles E, Jessell TM, Kaltschmidt JA. 2014. Neuronal Ig/Caspr recognition promotes the formation of axoaxonic synapses in mouse spinal cord. *Neuron* **81:** 120–129. doi:10.1016/j.neuron.2013.10.060

Bornstein B, Meltzer H, Adler R, Alyagor I, Berkun V, Cummings G, Reh F, Keren-Shaul H, David E, Riemensperger T, et al. 2021. Transneuronal Dpr12/DIP-δ interactions facilitate compartmentalized dopaminergic innervation of *Drosophila* mushroom body axons. *EMBO J* **40:** 1–21. doi:10.15252/embj.2020105763

Brovero SG, Fortier JC, Hu H, Lovejoy PC, Newell NR, Palmateer CM, Tzeng RY, Lee PT, Zinn K, Arbeitman MN. 2021. Investigation of *Drosophila* fruitless neurons that express dpr/dip cell adhesion molecules. *eLife* **10:** 1–69. doi:10.7554/eLife.63101

Carrillo RA, Özkan E, Menon KP, Nagarkar-Jaiswal S, Lee PT, Jeon M, Birnbaum ME, Bellen HJ, Garcia KC, Zinn K. 2015. Control of synaptic connectivity by a network of *Drosophila* IgSF cell surface proteins. *Cell* **163:** 1770–1782. doi:10.1016/j.cell.2015.11.022

Cosmanescu F, Katsamba PS, Sergeeva AP, Ahlsen G, Patel SD, Brewer JJ, Tan L, Xu S, Xiao Q, Nagarkar-Jaiswal S, et al. 2018. Neuron-subtype-specific expression, interaction affinities, and specificity determinants of DIP/Dpr cell recognition proteins. *Neuron* **100:** 1385–1400.e6. doi:10.1016/j.neuron.2018.10.046

Courgeon M, Desplan C. 2019. Coordination between stochastic and deterministic specification in the *Drosophila* visual system. *Science* **366:** eaay6727. doi:10.1126/science.aay6727

Enriquez J, Venkatasubramanian L, Baek M, Peterson M, Aghayeva U, Mann RS. 2015. Specification of individual adult motor neuron morphologies by combinatorial transcription factor codes. *Neuron* **86:** 955–970. doi:10.1016/j.neuron.2015.04.011

Eyjolfsdottir E, Branson S, Burgos-Artizzu XP, Hoopfer ED, Schor J, Anderson DJ, Perona P. 2014. Detecting social actions of fruit flies. In *Computer Vision—ECCV 2014. Lecture Notes in Computer Science, vol. 8690* (ed. Fleet D, et al.), pp. 772–787. Springer, Cham, Switzerland. doi:10.1007/978-3-319-10605-2_50

Gibson DA, Ma L. 2011. Developmental regulation of axon branching in the vertebrate nervous system. *Development* **138:** 183–195. doi:10.1242/dev.046441

Grueber WB, Sagasti A. 2010. Self-avoidance and tiling: mechanisms of dendrite and axon spacing. *Cold Spring Harb Perspect Biol* **2:** a001750. doi:10.1101/cshperspect.a001750

Guan W, Bellemin S, Bouchet M, Venkatasubramanian L, Guillermin C, Laurençon A, Kabir C, Darnas A, Godin C, Urdy S, et al. 2022. Post-transcriptional regulation of transcription factor codes in immature neurons drives neuronal diversity. *Cell Rep* **39:** 110992. doi:10.1016/j.celrep.2022.110992

Honig B, Shapiro L. 2020. Adhesion protein structure, molecular affinities, and principles of cell-cell recognition. *Cell* **181:** 520–535. doi:10.1016/j.cell.2020.04.010

Howard CE, Chen CL, Tabachnik T, Hormigo R, Ramdya P, Mann RS. 2019. Serotonergic modulation of walking in *Drosophila*. *Curr Biol* **29:** 4218–4230.e8. doi:10.1016/j.cub.2019.10.042

Hyman AA, Weber CA, Jülicher F. 2014. Liquid-liquid phase separation in biology. *Annu Rev Cell Dev Biol* **30:** 39–58. doi:10.1146/annurev-cellbio-100913-013325

Kondo N, Ueda Y, Kinashi T. 2024. Low-affinity LFA1-dependent outside-in signaling mediates avidity modulation via the Rabin8–Rab8 axis. *PNAS Nexus* **3:** 1–9. doi:10.1093/pnasnexus/pgae332

Lefebvre JL, Kostadinov D, Chen WV, Maniatis T, Sanes JR. 2012. Protocadherins mediate dendritic self-avoidance in the mammalian nervous system. *Nature* **488:** 517–521. doi:10.1038/nature11305

Lemieux M, Thiry L, Laflamme OD, Bretzner F. 2021. Role of DSCAM in the development of neural control of movement and locomotion. *Int J Mol Sci* **22:** 8511. doi:10.3390/ijms22168511

Morano NC, Lopez DH, Meltzer H, Sergeeva AP, Becker E, Bornstein B, Cosmanescu F, Schuldiner O, Honig B, Mann RS, Shapiro L. 2025. Members of the DIP and Dpr adhesion protein families use *cis* inhibition to shape neural development in

Downloaded from on October 9, 2025 - Published by Cold Spring Harbor Laboratory Press

Drosophila. *PLoS Biol* **23:** e3003030. doi:10.1371/journal.pbio.3003030

Moreland T, Poulain FE. 2022. To stick or not to stick: the multiple roles of cell adhesion molecules in neural circuit assembly. *Front Neurosci* **16:** 1–16. doi:10.3389/fnins.2022.889155

Mosca TJ, Luo L. 2014. Synaptic organization of the *Drosophila* antennal lobe and its regulation by the Teneurins. *eLife* **3:** e03726. doi:10.7554/eLife.03726

Özkan E, Carrillo RA, Eastman CL, Weiszmann R, Waghray D, Johnson KG, Zinn K, Celniker SE, Garcia KC. 2013. XAn extracellular interactome of immunoglobulin and LRR proteins reveals receptor-ligand networks. *Cell* **154:** 228–239. doi:10.1016/j.cell.2013.06.006

Rostam KD, Morano NC, Menon KP, Lopez DH, Shapiro L, Zinn K, Feng S, Mann RS. 2025. FETCH enables fluorescent labeling of membrane proteins in vivo with spatiotemporal control in *Drosophila*. *Proc Natl Acad Sci* (in press).

Sanes JR, Zipursky SL. 2020. Synaptic specificity, recognition molecules, and assembly of neural circuits. *Cell* **181:** 536–556. doi:10.1016/j.cell.2020.04.008

Schneider CA, Rasband WS, Eliceiri KW. 2012. NIH image to ImageJ: 25 years of image analysis. *Nat Methods* **9:** 671–675. doi:10.1038/nmeth.2089

Siebert M, Banovic D, Goellner B, Aberle H. 2009. *Drosophila* motor axons recognize and follow a sidestep-labeled substrate pathway to reach their target fields. *Genes Dev* **23:** 1052–1062. doi:10.1101/gad.520509

Sink H, Rehm J, Richstone L, Bulls YM, Goodman CS. 2001. Sidestep encodes a target-derived attractant essential for motor axon guidance in *Drosophila*. *Cell* **105:** 57–67. doi:10.1016/s0092-8674(01)00296-3

Stoeckli ET. 2018. Understanding axon guidance: are we nearly there yet? *Development* **145:** dev151415. doi:10.1242/dev.151415

Tadros W, Xu S, Akin O, Yi CH, Shin GJE, Millard SS, Zipursky SL. 2016. Dscam proteins direct dendritic targeting through adhesion. *Neuron* **89:** 480–493. doi:10.1016/j.neuron.2015.12.026

Tan L, Zhang KX, Pecot MY, Nagarkar-Jaiswal S, Lee P-T, Takemura S-Y, McEwen JM, Nern A, Xu S, Tadros W, et al. 2015. Ig superfamily ligand and receptor pairs expressed in synaptic partners in *Drosophila*. *Cell* **163:** 1756–1769. doi:10.1016/j.cell.2015.11.021

Telley L, Cadilhac C, Cioni JM, Saywell V, Jahannault-Talignani C, Huettl RE, Sarrailh-Faivre C, Dayer A, Huber AB, Ango F. 2016. Dual function of NRP1 in axon guidance and subcellular target recognition in cerebellum. *Neuron* **91:** 1276–1291. doi:10.1016/j.neuron.2016.08.015

Van Vactor D, Sink H, Fambrough D, Tsoo R, Goodman CS. 1993. Genes that control neuromuscular specificity in *Drosophila*. *Cell* **73:** 1137–1153. doi:10.1016/0092-8674(93)90643-5

Venkatasubramanian L, Guo Z, Xu S, Tan L, Xiao Q, Nagarkar-Jaiswal S, Mann RS. 2019. Stereotyped terminal axon branching of leg motor neurons mediated by IgSF proteins DIP-α and Dpr10. *eLife* **8:** 1–27. doi:10.7554/eLife.42692

Venken KJT, Schulze KL, Haelterman NA, Pan H, He Y, Evans-Holm M, Carlson JW, Levis RW, Spradling AC, Hoskins RA, et al. 2011. MiMIC: a highly versatile transposon insertion resource for engineering *Drosophila melanogaster* genes. *Nat Methods* **8:** 737–743. doi:10.1038/nmeth.1662

Xu S, Sergeeva AP, Katsamba PS, Mannepalli S, Bahna F, Bimela J, Zipursky SL, Shapiro L, Honig B, Zinn K. 2022. Affinity requirements for control of synaptic targeting and neuronal cell survival by heterophilic IgSF cell adhesion molecules. *Cell Rep* **39:** 110618. doi:10.1016/j.celrep.2022.110618

Downloaded from on October 9, 2025 - Published by Cold Spring Harbor Laboratory Press

A critical affinity window for IgSF proteins DIP-α and Dpr10 is required for proper motor neuron arborization

Davys H. Lopez, Kevin D. Rostam, Sumaira Zamurrad, et al.

Genes Dev. published online September 10, 2025
Access the most recent version at doi:10.1101/gad.352936.125

Supplemental Material https://genesdev.cshlp.org/content/suppl/2025/09/10/gad.352936.125.DC1

Published online September 10, 2025 in advance of the full issue.

Creative Commons License This article, published in *Genes & Development*, is available under a Creative Commons License (Attribution-NonCommercial 4.0 International), as described at http://creativecommons.org/licenses/by-nc/4.0/.

Email Alerting Service Receive free email alerts when new articles cite this article - sign up in the box at the top right corner of the article or **click here.**

Published by © 2025 Lopez et al.; Published by Cold Spring Harbor Laboratory Press